Applied Surface Science 425 (2017) 1066–1073

Contents lists available at ScienceDirect

Applied Surface Science

journal homepage: www.elsevier.com/locate/apsusc

Full Length Article

Indium local geometry in In-Sb-Te thin films using XANES and DFT calculations

V. Bilovol[a,b,*], A.V. Gil Rebaza[c,d], A.M. Mudarra Navarro[c], L. Errico[c,e], M. Fontana[a,b], B. Arcondo[a,b]

[a] Universidad de Buenos Aires. Facultad de Ingeniería. Departamento de Física. Laboratorio de Sólidos Amorfos. Paseo Colón 850, C1063ACV, Buenos Aires, Argentina
[b] CONICET-Universidad de Buenos Aires. Instituto de Tecnologías y Ciencias de la Ingeniería "Hilario Fernández Long" (INTECIN). Buenos Aires, Argentina
[c] Departamento de Física, Facultad de Ciencias Exactas de la Universidad Nacional de La Plata (UNLP), Instituto de Física La Plata, IFLP-CONICET, 1900, La Plata, Argentina
[d] Grupo de Estudio de Materiales y Dispositivos Electrónicos – GEMyDE, Facultad de Ingeniería, Universidad Nacional de La Plata, UNLP, 1900 La Plata, Argentina
[e] Universidad Nacional del Noroeste de la Provincia de Buenos Aires (UNNOBA), Monteagudo 2772, 2700, Pergamino, Buenos Aires, Argentina

ARTICLE INFO

Article history:
Received 1 March 2017
Received in revised form 19 June 2017
Accepted 8 July 2017
Available online 10 July 2017

Keywords:
In-Sb-Te
Amorphous films
Phase change memories
XANES
Dft

ABSTRACT

In-Sb-Te when is a thin film presents a huge difference in its electrical resistivity when transform from the amorphous (insulating) to the crystalline (conducting) phase. This property made this system one of the main phase-change materials used in the data storage industry. The change in the electrical conductivity is probably associated to a change in the bonding geometry of some of its constituents. To explore this point, we present in this work an study of the bonding geometry of In atoms in In-Sb-Te films by means of In *K*-edge X-ray absorption near edge structure (XANES) spectroscopy using synchrotron radiation in both *as deposited* (amorphous) and crystalline thin films obtained as a result of resistance (*R*) vs temperature (*T*) measurements. Comparison of the XANES spectra obtained for ternary amorphous films and binary crystalline reference films suggests that in amorphous films the bonding geometry of In atoms is tetrahedral-like. After the thermal annealing has been carried out the differences in the XANES spectra of the *as deposited* and the annealed films indicate that the bonding geometry of In atoms changes. Based on X-ray diffraction results and *ab initio* calculations in the framework of the Density Functional Theory (DFT) we show that the new coordination geometry is associated with a tendency of In atoms towards octahedral-like.

1. Introduction

The switching effect evidenced in phase change memory (PCM)-based materials made them very attractive candidates for applications in non-volatile memories' technology. Usually with the presence of a chalcogenide element (like, Te or Se) these materials reveal very interesting electrical properties depending on their structural characteristics. In particular, the electrical conductivity of this type of materials can change in a factor 10^7 when it transforms from the amorphous to the crystalline phase [1]. What makes these materials really valuables for applications in technology is a numerous cyclic recurrence transformation between low- and high-resistivity states with a high frequency. This phase transition also drastically affects the optical properties of the systems [2].

The knowledge of the coordination geometry of constitutive elements of the amorphous material is a key factor at the moment of understanding the amorphous-to-crystalline phase transition as well as to understand its main attractive properties. Many efforts were already put to understand this transition in the well-known $Ge_2Sb_2Te_5$ (GST) system [3,4]. It was shown that the local geometry of the Ge atom is different in amorphous and crystalline films. In particular, it was found that in the *as deposited* amorphous GST thin films the Ge atoms present tetrahedral geometry meanwhile after crystallization the geometry coordination of Ge atoms is octahedrally distorted. Moreover, it was shown that in GST amorphous film, Ge coordination geometry depends on the synthesis method. For example, in *as deposited* amorphous films prepared from the vapor phase, Ge sites are tetrahedrally coordinated, whilst laser- or

* Corresponding author at: Universidad de Buenos Aires. Facultad de Ingeniería. Departamento de Física. Laboratorio de Sólidos Amorfos. Paseo Colón 850, C1063ACV Buenos Aires, Argentina.
E-mail address: vbilovol@fi.uba.ar (V. Bilovol).

http://dx.doi.org/10.1016/j.apsusc.2017.07.063
0169-4332/

current pulsed-induced amorphous phase reveals pyramidal (alternatively referred as four-fold coordinated distorted octahedral) Ge sites [3,5]. On the other hand, the films produced by sputtering, present both distorted octahedral and tetrahedral Ge coordination [6].

Other system that exhibits the required properties for practical applications as a PCM is In_3SbTe_2 [7]. Both $Ge_2Sb_2Te_5$ and In_3SbTe_2 systems are structurally similar, crystallizing in a metastable cubic rocksalt type (NaCl) crystal structure [8]. In particular, the crystalline phase of In_3SbTe_2 is stable only in the temperature 470–570 °C range. At room temperature, crystalline In_3SbTe_2 is a metastable quasi-binary alloy that decomposes into InSb and InTe below 470 °C [9]. In the case of the ternary crystal, indium coordination geometry is known to be octahedral. For the binary phases, tetrahedral geometry for Indium is unique in InSb. In the case of InTe, there are two types of In atom sites. One of them is approximately tetrahedrally coordinated with four Te atoms whilst the second In atom is surrounded by eight Te atoms in a distorted square antiprismatic arrangement [10,11]. As for the structures of amorphous phases, their analysis is more complicated because of a lack of long-range order. The literature about In-Sb-Te is not as abundant as in Ge-Sb-Te case and experimental and theoretical studies of this system are still lacking.

Hereby, we will present an study of the system In-Sb-Te in the form of thin films obtained by pulsed laser deposition technique [12]. We focus our studies on the local geometry of In atom in both amorphous and crystalline films of two ternary eutectic compositions, $In_8Sb_8Te_{84}$ (E1 in the following) and $In_{10}Sb_{51}Te_{39}$ (E2). A third film with composition $In_{50}Sb_{15}Te_{35}$, called in advance IST, will be studied. IST presents a composition that is nearby that of the ternary compound In_3SbTe_2. The lack of long-range order in amorphous materials imposes limitations to the use of diffraction-based techniques that are typically used to probe structures. On the other hand, X-ray absorption near-edge spectroscopy (XANES) involving synchrotron radiation is very sensitive to three-dimensional order around specific atomic species. In consequence, XANES could give very valuable information about the local structure around a given atom in amorphous materials. Based on this, in the present work, we applied In K-edge spectroscopy to elucidate the local geometry and the changes induced by the thermal annealing around In atoms in both as deposited amorphous and crystalline E1, E2, and IST films. Traditionally, in order to identify the bonding geometry of a specific element in a sample, the analysis of the XANES results has been done by comparison with reference experimental spectra. In this sense, *ab initio* methods in the framework of the Density Functional Theory (DFT) [13] has been used to effectively evaluate XANES results (see, for example, Ref. [14–17] and references therein), because this methodology enables realistic electronic structure calculations including the core-hole effect produced in the XANES process. So, in order to better analyze the experimental XANES results realistic theoretical modeling of XANES spectra were performed.

2. Material and methods

2.1. Experimental

Bulk targets with nominal compositions $In_8Sb_8Te_{84}$ (E1), $In_{10}Sb_{51}Te_{39}$ (E2) and $In_{50}Sb_{15}Te_{35}$ (IST) were obtained by means of a melt quenching procedure of the elemental components contained in previously evacuated quartz ampoules as was described in [12]. The bulk targets were underwent an ablation process employing a pulsed Nd:YAG laser (λ = 355 nm) and deposited as films on either standard microscope glass substrates or Si wafers. The final composition of the films is in agreement with those of the targets

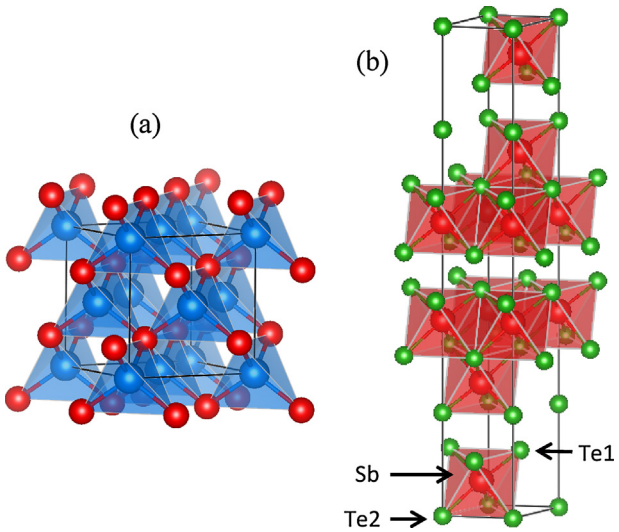

Fig. 1. Crystal structure of a) InSb and b) Sb_2Te_3 compounds. Blue, red and green balls represent In, Sb and Te atoms, respectively. (For interpretation of the references to colour in this figure legend, the reader is referred to the web version of this article.)

though a low chalcogen loss takes place due to its relatively high vapor pressure. Te loss is about 1% for E1, 2% for E2 and 3% for IST. Similar results were reported by other authors [18,19]. The structural characteristics of the In-Sb-Te *as deposited* films as well as those of the crystalline phases observed after thermal annealing were established by XRD [12].

InSb and InTe crystalline films were grown with the same technique and methodology described above with the goal to use them as XANES references in subsequent analysis.

Thermal annealing of the as-deposited films was achieved by measuring resistivity vs temperature curves. The heating, performed in vacuum, is well fitted with sigmoidal T vs t curves (Boltzmann type) up to the maximum temperature, followed by a free cooling into the measurement cell (exponential decay). After the first minutes, on heating, the heating rate is nearly constant and of about 30 °C/min.

XANES measurements at the In K-edge were performed at room temperature in fluorescence mode using X-ray Diffraction and Spectroscopy beamline of Laboratório Nacional de Luz Síncrotron (Campinas, Brazil). The XANES data analysis was performed using *Athena* software (version 0.8.056) by subtracting a linear background and rescaling the absorbance by normalizing the difference between the baseline and the post-edge absorption.

2.2. Electronic structure calculation

For the interpretation of our experimental XANES results, we have performed *ab initio* calculations using the full-potential linearized augmented plane wave method (FP-LAPW) [20] in order to obtain the electronic structure of relevant reference compounds, namely, InSb and In doped-Sb_2Te_3 (see ref. [12]), and from it the theoretical XANES spectra were obtained. In Fig. 1, the crystal structures for the InSb and Sb_2Te_3 compounds are shown. InSb has a cubic crystal structure with space group $F\text{–}43m$ (216) and lattice parameter $a = 6.1100$ Å [21], the In and Sb atoms are located at the positions (0, 0, 0) and (1/4, 1/4, 1/4), respectively, corresponding to the *4a* and *4c* Wyckoff positions. Both atoms present a tetrahedral coordination, see Fig. 1(a). Sb_2Te_3 crystallizes in a rhombohedral crystal structure with space group $R\text{–}3m$ (166) and lattice parameters $a = b = 4.264$ Å and $c = 30.458$ Å [21]. This structure is characterized by three non-equivalent crystallographic sites: Sb, Te1 and Te2. Sb is located in the *6c*:(0,0,u) position, whilst

Te1 and Te2 are located at *6c*:(0,0,*v*) and *3a*:(0,0,0) Wyckoff positions, respectively. *u* and *v* are internal parameters with values *u* = 0.39880 and *v* = 0.78720. In this structure Sb and Te sites present an octahedral coordination, see Fig. 1(b).

In order to determine the site that the impurity-In atom occupies in the Sb_2Te_3 host we have performed *ab initio* total energy calculations using the supercell (SC) method. Calculations were made for a periodic SC of $2 \times 2 \times 1$ of Sb_2Te_3. The resulting SC has dimensions $a' = b' = 2a = 8.5280$ Å, $c' = c = 30.4580$ Å. We have considered that the In atom could occupy the three possible crystallographic sites, Sb (*6c*), Te1 (*6c*) and Te2 (*3a*) and for each case we determine the energies of the systems. In all cases, the structural distortions induced by the In impurity in the host systems were also computed. In order to estimate the preferred site occupation, we compared the defect formation energies, i.e. the substitution energies, E_{subst}, for all sites using the expression:

$$E_{subst} = E^{tot}_{subst} - E^{In} + E^{X} - E^{pure} \quad (1)$$

Here E^{tot}_{subst} is the total energy of the SC containing a single substitutional In atom, E^{In} and E^{X} denote the energies of an In impurity and Sb or Te atoms, and E^{pure} is the energy of the SC without impurities. E^{In} and E^{X} were obtained from metallic In, Sb and Te with the same precision as that in the doped SC. In passing we note that small values of the substitution energies indicate preferential replacement of a native atom by an Indium impurity.

All calculations presented here were performed with the Wien2k code [22], an implementation of the FP-LAPW method. The exchange-correlation potential was treated within the Generalized-Gradient Approximation (GGA) with the parametrization of Perdew–Burke–Ernzerhof (PBE) [23]. The muffin-tin radii (R_{MT}) used for In, Sb, and Te were 1.30 Å and the $R_{MT} \times K_{max}$ parameter (which controls the size of the basis set) was set to 9.0, where R_{MT} is the smallest muffin-tin radius and K_{max} is the largest wavenumber of the basis set. Integration in the reciprocal space was performed using the tetrahedron method taking up to 182 *k-points* in the First Brillouin Zone. Several convergence tests showed that, for these parameters, the obtained results are extremely well converged.

For the calculations of the XANES spectra we considered two cases that were computed separately: the ground state and the transition state that is characterized by the excitation of an 1*s*-In core electron to an unoccupied *5p*-In band (core-hole correlation [17]). This hole in the core states of the probe atom influences the electronic structure of the system and this perturbation must be taken into account in the calculation of the XANES spectra. Similarly to other works [14,17,24] calculations in which the core-hole effect is not included predict XANES spectra that are far from being satisfactory in reproducing the experimental results. In the present calculations the core-hole effects were fully taken into account by removing one electron from the 1*s*-In state and adding one electron as a uniform charge background.

Due to periodic boundary conditions, $2 \times 2 \times 2$ and $2 \times 2 \times 1$ SCs were considered for InSb and Sb_2Te_3, respectively, in order to minimize spurious interactions between adjacent core-holes. For these SCs the minimum distance among adjacent atoms with core-hole is at least 9 Å. Although a small interaction cannot be excluded, such separation is typical of FP-LAPW calculations including the core-hole correction [14,15,17], such as MgO [25], Li_2O [26] and other systems that contains transition metals atoms [27]. Theoretical XANES spectra were obtained by a product of the projected partial density of state (PDOS) for unoccupied 5*p* orbitals in the final state and the radial part of the transition matrix elements. A Gaussian broadening of 1.0 eV (full width at half maximum) was included in the calculation of the PDOS.

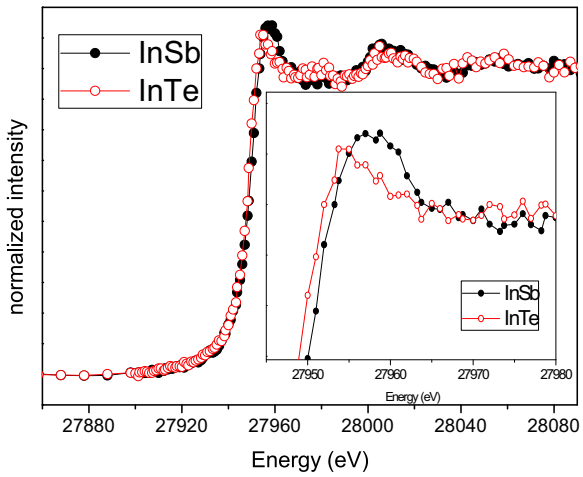

Fig. 2. In *K*-edge XANES spectra of crystalline InSb and InTe films used as reference standards. Inset: zoom of the top part of the absorption jumps.

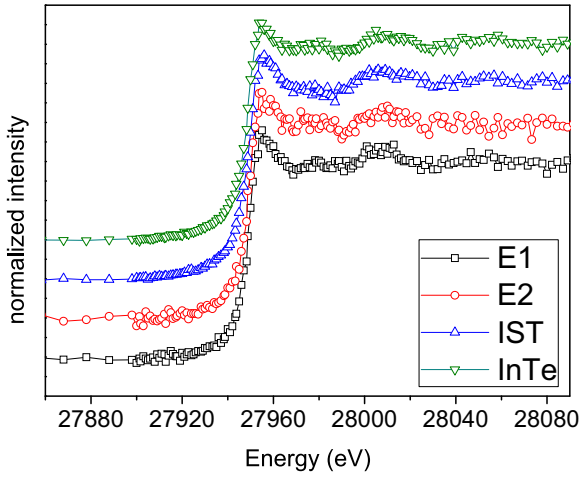

Fig. 3. In *K*-edge XANES spectra of as deposited (amorphous) E1, E2, IST films. XANES spectrum of InTe film is also shown as a reference.

3. Results

Fig. 2 shows In *K*-edge experimental XANES spectra of crystalline InSb and InTe films used as reference standards. As it can be appreciated, the XANES spectra of the binary compounds are very similar, although a slight difference is observed when magnifying the top part of the XANES curves. A more detailed discussion about the similarities and differences between these XANES spectra will be presented in Section 4.

Fig. 3 clearly demonstrates the similarity of the XANES spectra of *as deposited* E1, E2 and IST amorphous films (the spectra are intentionally shifted in vertical axes). This similarity points to a similar coordination geometry of the In-probe atoms in all studied *as deposited* films. On the other hand, these spectra are similar to the ones of the binary crystalline films taken as the reference standard. This unambiguously indicates that the In atoms present similar bonding geometry coordination in all the films.

XANES spectra of *as deposited* (amorphous) and corresponding annealed E1, E2 and IST films are shown, for a comparative purpose, in Fig. 4. In all cases clear differences between XANES spectra of the *as deposited* and annealed films can be seen. In the following, these differences will be referred to as “features”. Feature 1 is an increase of the intensity of the absorption edge observed weakly in IST film, moderately in E2 film and strongly in E1 film. Feature 2 is

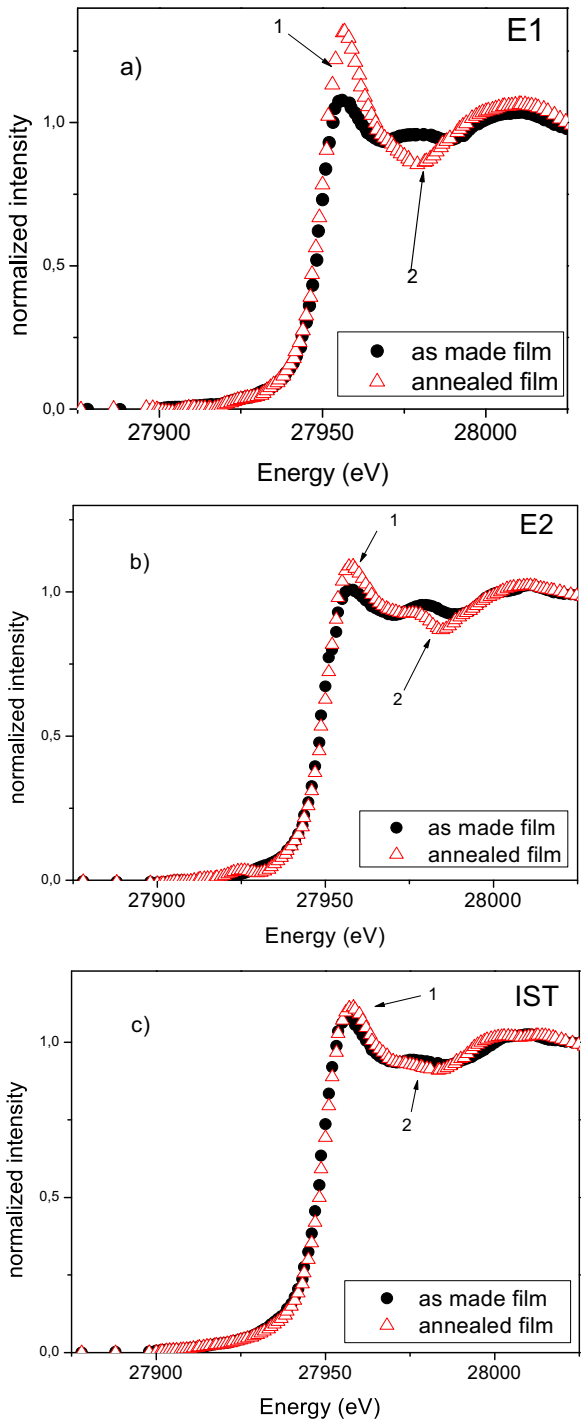

Fig. 4. In *K*-edge XANES (smoothed) spectra of amorphous and thermally annealed: (a) E1, (b) E2 and (c) IST films. The main differences after thermal annealing of the films are: feature 1: change in absorption intensity; feature 2: disappearance of 27980 eV- resonant line.

a tendency towards disappearance of the 27980 eV – resonant line in the annealed films, especially evident in E1.

4. Discussion

It is well known that InSb crystallizes in a ZnS-type crystal structure (*F–43 m* space group) [21]. In such a structure, the In atoms with 3+ oxidation state are in a unique crystallographic site with a tetrahedral coordination (In atoms has four Sb atoms as first neighbours). On the other hand, InTe crystallizes in a TlSe-type crystal structure (*I4/mcm* space group) [11]. In this case the metal atom adopts two equally abundant crystallographic sites: *In1* atom (with 3+ oxidation state) located in the *4b* Wyckoff position is tetrahedrally coordinated by four chalcogen (Te) atoms at 2.819 Å; *In2* atom (with 1+ oxidation state) located in the *4a* Wyckoff position is surrounded by a "cage like" (antiprismatic) system of 8 chalcogen atoms at 3.576 Å and two *In2* atoms at the same distance located symmetrically along the *c* axis [10,11]. Both units form chains along the *c* axis but while $In1^{3+}$ tends to form covalent bondings, the $In2^{1+}$ tends to form bonding with a larger ionic character [28]. Although the local geometry of *In2* atom is very different from that of *In1* atom this peculiarity does not correlate to a very remarkable contribution to the XANES curve of InTe film, as can be seen in Fig. 2. That is, the *In2*-Te contribution to the intensity of the XANES curve has been smeared out. In order to understand this fact, we can refer to the results reported in reference 11. In that work the authors reported an Extended X-Ray Absorption study at the Se K-edge in an $InTe_{0.8}Se_{0.2}$ sample (Se substitutes Te in the solid solution). In this system the second shell of the Se atoms consists of four atoms in *In2* positions and is characterized by a very large Debye-Waller factor (σ^2), so is strongly smeared out. Additionally, a notable contribution of the third shell formed by the closest chalcogen atoms in the cage was reported. This fact is attributed to the weak chemical bond between a *In2* atom and chalcogen neighboring atoms, and can be applied to understand why mainly *In1* (tetrahedral coordination) contributes to the XANES spectra obtained in our study.

X-ray absorption process involves an electronic transition from a (filled) core level to an empty state. The transition (a dipole transition to a first order) is allowed, according to the selection rule, for $\Delta l = \pm 1$. In such a way, measuring absorption at the K-edge of In, we promote $1s \rightarrow 5p$ electronic transition in the In-probe atom. Generally, the occupancy of *p* states influences the absorption peak height being an indication of empty density of states (EDOS). As it was observed from XANES experimental curves, the intensity of the absorption curve for Indium in the tetrahedral sites is smaller than that of those corresponding to the octahedral sites [29]. This is an indication of lower EDOS in tetrahedral sites, comparing it with EDOS in octahedral sites. This is because in tetrahedral geometry the bond-lengths are shorter, strongly affecting the occupancies of *p* states of absorbing atom due to sp^3 hybridization. In the literature the term "octahedral-like" is used when referred to defective octahedral site (5, 4, 3-fold site). One of the main differences between tetrahedral and defective octahedral sites consists in slightly longer bond lengths for the latter ones. Besides, bond angles close to 90° are characteristic of octahedral-like sites, whilst bond angles about 109° are the characteristic ones of tetrahedral sites [30].

As we reported earlier, all three *as deposited* films prepared by pulsed laser deposition technique resulted amorphous as it was shown by XRD technique [12]. Qualitative analysis (by comparison with the references) of the experimental spectra shown in Fig. 3 suggests that In atoms in all *as deposited* amorphous films are in tetrahedral-like bonding geometry. Similar XANES features of In coordination geometry were thorough studied for the same probe-atom in aqueous complexes [29] and unambiguously attributed to tetrahedral environment.

One common characteristic of the three as deposited films is their highly resistive behavior. This fact can be understood in the framework of a simple model proposed by Mott and Davies [31]. Chalcogenide glasses appear to obey the 8-N rule whatever the composition. That is, the coordination number of an atom depends on its number of outer electrons (N) as 8-N. However, if constituents with less than four outer electrons are present, they may form four bonds and may probably be negatively charged [31]. In our case, Sb may be coordinated by three atoms, Te by two and In four-fold coordinated and, occasionally, negatively charged with an

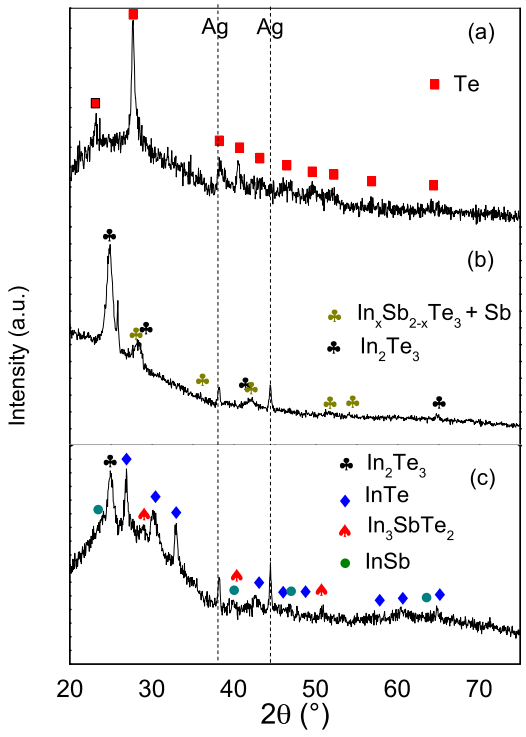

Fig. 5. XRD patterns, obtained at room temperature, from thermally annealed films (a) E1, (b) E2, (c) IST. The presence of Ag is due to rests of electric contacts on the films. Taken from ref. [12].

electron provided by an ionic In^{+1} or by structural defects (i.e. dangling bonds). These characteristics are compatible with the highly resistive behavior of these as prepared glasses.

After *as deposited* amorphous films have been submitted to thermal annealing as a result of *R vs T* measurements, their crystallization was corroborated by XRD as it has been previously reported [12] (see Fig. 5). On the other hand, both XRD and XANES techniques make evident structural changes in the films after thermal energy has been provided to them. The changes are not only of a long-range order but of a short-range (local) as well. The most evident changes in the In K-edge XANES spectra come as feature 1 and 2 in all three films (see Fig. 4). In accordance with other experimental studies reported in the literature [29,32], these differences could be attributed to a change of the local geometry of In: a change from tetrahedral to octahedral-like coordination. In order to better describe the In environments, we will analyzed each film separately.

E1 film: The most prominent change of the XANES spectra of the annealed E1 film with respect to the as deposited film (octahedral-like geometry for In atom is highly dominant in the annealed E1 film, see Fig. 4a) can be explained as it follows. We found that E1 film crystallized in Te phase ($P3_121$ space group) with the lattice constants *a* and *c* slightly reduced. As a consequence, the volume of the cell is about 2% smaller as it was compared with pure Te bulk sample. Since Te atoms in Te phase are located in sites with octahedral geometry (Fig. 6a), we suggest that In atoms are solute in the Te phase, replacing the octahedrally coordinated Te atoms (Fig. 6b). In order to corroborate this, we performed ab initio simulation of the XANES spectrum at the In K-edge of In-doped Te (4 at% of In doping, see Fig. 6b). On the other hand, as a reference for tetrahedrally coordinated In, we simulated the XANES spectrum at the In K-edge of In atoms in the InSb compound. At this point we have to mention that the comparison *ab initio* calculations-experiment will be qualitative, even though they reveal the main features of local geometries. Besides numerical errors and the intrinsic error introduced due to the functional employed for the exchange and correlation functional (we verified that these errors are not significant), different approximations are a source of a deviation between theory and experiment. DFT is a ground-state theory, so it should fail for the prediction of excited state properties. However, for some systems and properties it works pretty well. In the case of X-ray absorption properties, only the XANES region (few tens of eV above the Fermi level) can be accurately calculated. Other source of error in our calculations is related to the core-hole correction. In order to avoid (spurious) interactions between core-hole corrections, a supercell is required. The question at this point is the size of the supercell needed for the calculation (larger supercells give better results but implies larger computational time and resources). In our case, the core-hole separation is in the order of 9 Å, so we can discard significant errors associated to the supercell size in our results. Finally, we have to take into account that we are comparing amorphous films with the XANES spectra predicted for crystalline references. This approach gives us qualitative information that enables the interpretation of our results but to go further and to obtain a better agreement between the calculated XANES spectra and the experimental ones, a more refined model will be necessary.

In Fig. 6c we present the FP-LAPW prediction for the In K-edge XANES spectra of In-doped Te (octahedral In coordination) and InSb (tetrahedral In coordination). For a simple comparison the XANES spectra of the as deposited E1 film is also included. As can be seen, the simulated XANES spectra at the In K-edge in both bonding geometries reflect the main features of the corresponding experimental results (Fig. 4a): a higher white peak intensity for octahedral geometry and absence of a shoulder on its right (that is proper of tetrahedral geometry). From Fig. 6c we can conclude that the experimental spectrum is qualitatively well reproduced by the simulated InSb spectrum.

In Fig. 6d we compare the same theoretical spectra with the experimental XANES results for the annealed E1 film. In this case, it is clear that the simulated XANES spectrum of In diluted in Te phase is in very good agreement with the XANES spectrum of thermally annealed E1 film.

In conclusion, the change of the XANES spectrum of E1 film after annealing treatment (a manifestation of change of bonding geometry of In atom) can be associated with the In solute in Te phase. On one hand, we have identified this phase in the XRD pattern of annealed E1 film (Sb solute in Te phase is also assumed, [12]). On the other hand, In in a 3+ charge state, doping $Pb_{0.78}Sn_{0.22}Te$, has been reported by Aleksandrov et al. [33] for In concentration between 0.7-0.8 mol%. In this case, In atoms are surrounded by Te atoms in an octahedral type coordination involving ionic In-Te bonds. Reinforcing these evidences, the first-principles study indicates that In atom should have octahedral-like geometry after the annealing treatment. This is indicative of a loss of directionality of the bonds [34,35], when it is dissolved in pure tellurium.

E2 film: One of the crystalline phases identified in E2 film after R vs T measurements is Sb_2Te_3. As it was reported in Refs. [36,37] and mentioned by us in [12], Sb_2Te_3 phase admits an important solubility of In_2Te_3. In such a case In atom should be substitutionally located at the Sb site. Here, in order to get more evidences that confirm this assumption, we performed a first-principles study of the Sb_2Te_3 compound where Sb is in octahedral environment and there are two non-equivalent sites for Te (*Te1* and *Te2*) [10]. For the calculations we considered separately the possible scenarios: In-impurities replacing Sb, In replacing Te1 and In replacing Te2. Taking into account the maximum In_2Te_3 solubility in Sb_2Te_3 at room temperature [37], we adopted the following systems for the calculations: i) the In atom occupies the Sb site ($In \rightarrow Sb$) forming $In_{0.33}Sb_{1.67}Te_3$ compound, ii) and iii) the In atom occupies one of Te sites ($In \rightarrow Te1$ or $In \rightarrow Te2$) forming $In_{0.33}Sb_2Te_{2.67}$ compound.

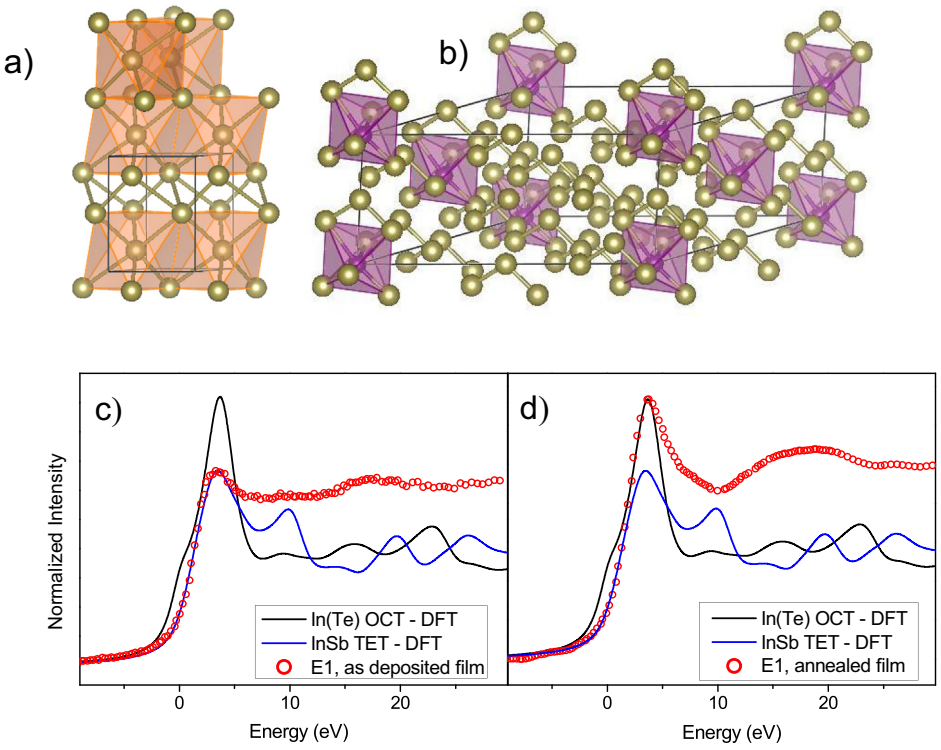

Fig. 6. Crystal structure of a) Te; b) In-doped Te (4 at.%). The big/small balls represent Te/In atoms; (c) FP-LAPW simulated In K-edge XANES spectra of In-doped Te (4 at.%, octahedral In coordination) and InSb (tetrahedral In coordination). For the sake of comparison the experimental In K-edge XANES spectrum of as-deposited E1 film is shown. (d) Ibid (c) but now the experimental XANES spectrum corresponds to the thermally annealed E1 film.

Table 1
ab initio predictions for the substitution energies for an In atom in the Sb_2Te_3 structure.

	$In_{0.33}Sb_{1.67}Te_3$	$In_{0.33}Sb_2Te_{2.67}$ In at Te1 site	$In_{0.33}Sb_2Te_{2.67}$ In at Te2 site
ΔE (meV)	−166.46	1094.13	1324.37

For each case all atomic positions were optimized and the energy of substitution was calculated using equation (1). The results for the substitution energies can be found in Table 1. From this, we conclude that In atom substitution for Sb is favored rather than substitution for Te.

Then, we simulated the XANES spectrum at the In K-edge of the $In_{0.33}Sb_{1.67}Te_3$ structure where In atom is located in octahedral geometry, as it was mentioned before. Fig. 7 shows the simulated XANES curves for In in $In_{0.33}Sb_{1.67}Te_3$ together with that of In in InSb, already presented in Fig. 6c and the experimental In K-dge XANES spectrum of the thermal annealed E2 film. The simulated XANES curves at the In K-edge in both bonding geometries reflect rather reasonably the main features of the corresponding experimental one.

The XANES spectrum of E2 film after annealing treatment can be mainly associated with the $In_xSb_{(2-x)}Te_3$ phase. On one hand, we have identified this phase as it is expected from the corresponding phase diagram [37] in the XRD pattern of annealed E2 film [12]. On the other hand, the first-principles study indicates that In atom should have octahedral-like geometry when it is dissolved in antimony telluride compound. Nevertheless, In_2Te_3 compound has also been identified in annealed E2 film (see Fig. 5b). As it was reported by Madelung [38], In_2Te_3 has a zinc blende structure with In atoms in tetrahedral coordination. Since XANES technique gives information about average local geometry of all In atoms, the XANES curve obtained for E2 annealed film averages two contributions

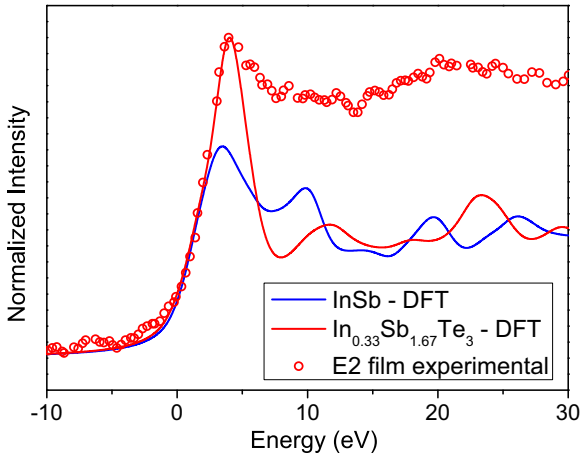

Fig. 7. FP-LAPW XANES In K-edge spectra of $In_{0.33}Sb_{1.67}Te_3$ and InSb. For the sake of comparison the experimental In K-edge XANES spectrum of the annealed E2 film is also shown.

and one of them, that corresponding to In_2Te_3, is "responsible" for that characteristics associated with In in octahedral coordination lose relevance as compared with E1 film.

There is a last point to discuss here. As can be seen in Fig. 4b, a weak peak at nearly 27925 eV is observed. A similar pre-edge structure was observed in the case of Al K-edge XANES studies of Al^{3+} goethite [39]. The peak was attributed to a 1s → 3 s electronic transition. Similarly, for the case of In^{3+}, the peak we observed can be attributed to a 1s → 5 s electronic transition. Atomic calculations of the In energy levels confirms this conclusion.

IST film: In the diffractogram of the crystalline IST film, traces of In_3SbTe_2 phase were found in addition to InSb and InTe. In_3SbTe_2 ternary compound has a NaCl-type cubic structure (*Fm–3 m* space

group) where In atoms and vacancies occupy the Na sites while Sb, Te and vacancies occupy the Cl sites [10]. In such a structure In atoms in *4a* Wyckoff position have octahedral-like bonding geometry. As was already mentioned for E2, due to the coexistence of In in tetrahedral and octahedral-like environments, the resulting experimental XANES spectrum is a weighted average of both In-coordinations. On the basis of the qualitative analysis of the X-ray diffractogram of thermally treated IST film, we conclude that a slight change of the bonding geometry around In atoms can be explained by, at least, the presence of the crystalline cubic ternary In_3SbTe_2 phase in which the In atoms are located in sites with octahedral-like geometry.

Summarizing, when *as deposited* films were crystallized during R vs T measurement [12], a qualitative change of the annealed XANES spectra was observed: the absorption edge intensity of XANES curve (feature 1) increased while the resonance at nearly 27980 eV (feature 2), characteristic of tetrahedral-like coordination geometry, reduced its intensity. These features are associated with an octahedral-like geometry of In atom (in agreement with already mentioned references 29 and 31). In particular, a very large fraction of In atoms in the E1 film, most of which were tetrahedrally coordinated in the *as deposited* amorphous films, changed its short range order towards octahedral-like coordination when crystallization took place. On the other hand, this is not the case either for E2 or for IST. Accordingly, those features that are the signature of octahedral coordination for In, are particularly strong in the XANES curve of annealed E1 film as compared with those of E2 and IST.

Finally, the change from tetrahedral to octahedral type coordination of In is an indication of a loss of directionality of In bonds which may add an extra improving of electrical conductivity upon crystallization.

Now, the evaluation of the resistivity results reported in [12] is performed in the framework of the above description, that is, structure-properties correlation is evaluated.

E1 sample crystallization takes place at about 135–145 °C with a fall of $\log(\rho_r)$ of more than one order of magnitude. This jump may be attributed to the change in cation geometry from tetrahedral to octahedral. All cation environments result octahedral upon crystallization, particularly all In environments. Cation concentration (In + Sb) is 16 mol%.

E2 sample crystallization takes place at about 200–225 °C with a fall of $\log(\rho_r)$ of about two orders of magnitude. This fact may be attributed to the change of the cation (In, Sb) geometries towards octahedral geometry. However the presence of In in tetrahedral sites at In_2Te_3 is also observed. The relative amount of both compounds ($In_xSb_{2-x}Te_3/In_2Te_3$) can be estimated. For example, asuming x = 0.33 as before, their relative fraction is about 2.8. In this case, it results that the crystallized sample is formed by 47.9 mol% of $In_{0.33}Sb_{1.67}Te_3$, with cations in octahedral environments, 17.1 mol% of In_2Te_3, with cations in tetrahedral environments, and 35 mol% of metallic Sb. As a consequence, the major fall in resistivity $\log(\rho_r)$, in this sample, may be attributed to cations (In, Sb) in octahedral environments plus the simultaneous presence of metallic Sb. The relative weight of each contribution depends on temperature.

IST as prepared sample has a strong dependence of $\log(\rho_r)$ on temperature, however the change of ρ_r upon crystallization at about 310–330 °C is not remarkable. This fact may be attributed to the similarity of the cation (In) environments either in amorphous or in crystalline phases (InSb and InTe). Indium has tetrahedral environments in all of them. After the solid state reaction that begins at about 380–400 °C, where In3SbTe2 is formed, a decreasing jump of one order of magnitude in $\log(\rho_r)$ takes place. This fall may be attributed to the change of the local geometry around cation, from tetrahedral to octahedral. A last change takes place above 450 °C where the resistivity regime turns to be metallic.

5. Conclusions

Indium bonding geometry in *In-Sb-Te* thin films, *as deposited* and after their thermal annealing, was analyzed by XANES technique using synchrotron radiation. It was verified that in all semiconductor (at room temperature) *as deposited* amorphous films under study (with 8, 10 and 50 at.% of *In*), In atoms are predominantly in sites with tetrahedral-like coordination geometry (similar to the case of Ge atom in GST films). After annealing treatments a change from tetrahedral-like to octahedral-like coordination was observed. This change was explained on the base of the XRD results obtained for the annealed films. *Ab initio* calculations reinforce our interpretation of the experimental data. As the cation coordination may be associated to the band structure, including the band gap, without entering into the analysis of each particular composition, the key of the remarkable jump in resistivity upon crystallization [12] may be the switching between their tetrahedral and octahedral coordination.

Acknowledgement

We are grateful to LNLS: Campinas, Brazil (project XDS-19052) for the partial financial support. We thank Universidad de Buenos Aires (Project 20020130100647BA), CONICET (PIP 11220120100541) and ANPCyT (PICT08-1314) for their financial support.

References

[1] S. Raoux, G.W. Burr, M.J. Breitwisch, C.T. Rettner, Y.-C. Chen, R.M. Shelby, M. Salinga, D. Krebs, S.-H. Chen, H.-L. Lung, C.H. Lam, Phase-change random access memory: a scalable technology, IBM J. of research and development 52 (4/5) (2008) 465–478.
[2] Guoxiang Wang, Chao Li, Daotian Shi, Qiuhua Nie, Hui Wang, Xiang Shen, Yegang Lu Controllable crystal growth and fast reversible crystallization-to-amorphization in Sb_2Te-TiO_2 films, Sci. Rep. 7 (2017) 46279.
[3] M. Krbal, A.V. Kolobov, P. Fons, J. Tominaga, S.R. Elliot, J. Hedegus, T. Uruga, Intrinsic complexity of the melt-quenched amorphous $Ge_2Sb_2Te_5$ memory alloy, Phys. Rev. B 83 (2011) 054203.
[4] A.V. Kolobov, M. Krbal, P. Fons, J. Tominaga, T. Uruga, Distortion-triggered loss of long-range order in solids with bonding energy hierarchy, Nat. Chem. 3 (2011) 311–315.
[5] M. Krbal, A.V. Kolobov, P. Fons, K.V. Mitrofanov, Y. Tamenori, J. Hegedus, S.R. Elliot, J. Tominaga, Selective detection of tetrahedral units in amorphous GeTe-based phase change alloys using Ge L_3-edge x-ray absorption near-edge structure spectroscopy, Appl. Phys. Lett. 102 (2013) 111904.
[6] S. Caravati, M. Bernasconi, T.D. Kühne, M. Krack, M. Parrinello, Coexistence of tetrahedral- and octahedral-like sites in amorphous phase change materials, Appl. Phys. Lett. 91 (2007) 171906.
[7] L. Men, F. Jiang, F. Gan, Short-wavelength phase-change optical data storage in In-Sb-Te alloy films, Mater. sci. Eng.: B 47 (1997) 18–22.
[8] V.L. Deringer, W. Zhang, P. Rausch, R. Mazzarello, R. Dronskowki, M. Wuttig, A chemical link between Ge-Sb-Te and In-Sb-Te phase-change materials, J. Mater. Chem. C 3 (37) (2015) 9519–9523.
[9] K. Deneke, A. Rabenau, Über die Natur der Phase In_3SbTe_2 mit Kochsalzstruktur, J. Inorg. Gen. Chem. 333 (4–6) (1964) 201.
[10] J.H.C. Hogg, H.H. Sutherland, Indium Telluride, Acta Crystallogr. 32 (1976) 2689.
[11] A.I. Lebedev, A.V. Michurin, I.A. Sluchinskaya, V.N. Demin, I.H.Munro EXAFS and electrical studies of new narrow-gap semiconductors: $InTe_{1-x}Se_x$ and $In_{1-x}Ga_xTe$, J. Phys. Chem. Solids 61 (2000) 2007–2012.
[12] V. Bilovol, B. Arcondo, Exploring the applicability of amorphous films of system In-Sb-Te as phase change materials, J. Non-Cryst. Solids 447 (2016) 315–321.
[13] P. Hohenberg, W. Kohn, Inhomogeneous electron gas, Phys. Rev. 136 (1964) B864;
W. Kohn, L.J. Sham, Self-consistent equations including exchange and correlation effects, Phys. Rev. 140 (1133) (1965).
[14] C. Suzuki, T. Nishi, M. Nakada, M. Akabori, M. Hirata, Y. Kaji, Core-hole effect on XANES and electronic structure of minor actinide dioxides with fluorite structure, J. Phys. Chem of Solids 73 (2012) 209 (and references there in).
[15] I. Tanaka, T. Mizoguchi, First-principles calculations of x-ray absorption near edge structure and energy loss near edge structure: present and future, J. Phys.: Condens. Matter 21 (2009) 104201.
[16] S. Nakashima, K. Fujita, K. Tanaka, K. Hirao, T. Yamamoto, I. Tanaka, First-principles XANES simulations of spinel zinc ferrite with a disordered cation distribution, Phys. Rev B 75 (2007) 174443.

[17] Vincent Mauchamp, Michel Jaouen, Peter Schattschneider, Core-hole effect in the one-particle approximation revisited from density functional theory, Phys. Rev. B 79 (2009) 235106.
[18] T. Schröder, T. Rosenthal, S. Grott, C. Stiewe, J. de Boor, O. Oeckler, Disorder and transport properties of In_3SbTe_2–an X-ray, neutron and electron diffraction study, Z. Anorg. Allg. Chem. 639 (14) (2013) 2536.
[19] L. Hromádko, J. Prikryl, L. Strizík, P. Koštál, L. Beneš, M. Frumar, Physico-chemical properties of Sb-rich (Sb, In)-Te thin films, J. Alloys Compd. 617 (2014) 306.
[20] E. Sjöstedt, L. Nordström, D.J. Singh, Alternative way of linearizing the augmented plane-wave method, Solid State Commun. 114 (15) (2000); G.K.H. Madsen, P. Blaha, K. Schwarz, E. Sjöstedt, L. Nordström, Efficient linearization of the augmented plane-wave method, Phys. Rev. B 64 (195134) (2001); S. Cottenier, Density Functional Theory and the Family of (L)APW-Methods: A Step-by-Step Introduction, KU Leuven, Belgium, 2002.
[21] http://www.crystallography.net/.
[22] P. Blaha, K. Schwarz, G. Madsen, D. Kvasnicka, J. Luitz, in: K. Schwarz (Ed.), WIEN2k, An Augmented Plane Wave Plus Local Orbitals Program for Calculating Crystal Properties, Technical Universität, Wien, Austria, 1999.
[23] J.P. Perdew, K. Burke, M. Emzerhof, Generalized gradient approximation made simple, Phys. Rev. Lett 77 (1996) 3865.
[24] Yun Mui Yiu, Gurinder Kaur, Qunfeng Xiao, Tsun Kong Sham, Ab-initio calculation of the As and Se $L_{3,2}$-edge XANES of As_2Se_3 and Zn-doped As_2Se_3 and comparison to the experiments, J. Non-Cryst. Solids 364 (2013) 13–19.
[25] Nan Jiang, Dong Su, C.H. John Spence, Comparison of Mg L23 edges in MgO and Mg(OH)2–importance of medium-range structure, Ultramicroscopy 109 (2008) 122–128.
[26] N. Jiang, J.C.H. Spence, Core-hole effects on electron energy-loss spectroscopy of Li_2O, Phys. Rev. B 69 (2004) 115112.
[27] C. Hébert, J. Luitz, P. Schattschneider, Improvement of energy loss near edge structure calculation using Wien2k, Micron 34 (2003) 219.
[28] Mixed or Intermediate Valence Group 13 Metal Compounds, B.F.T. Cooper and C.L.B. Macdonald in The Group 13 Metals Aluminium, Gallium, Indium and Thallium: Chemical Patterns and Peculiarities; Editors: Simon Aldridge y Anthony J. Downs, John Wiley & Sons, Ltd. 2011, p. 364.
[29] Hirokazu Narita, Mikiya Tanaka, Hideaki Shiwaku, Yoshihiro Okamoto, Shinichi Suzuki, Atsushi Ikeda-Ohno, Tsuyoshi Yaita, Structural properties of the inner coordination sphere of indium chloride complexes in organic and aqueous solutions, Dalton Trans. 43 (2014) 1630.
[30] J.H. Los, Th.D. Kuhne, S. Gabardi, M. Bernasconi, First-principles study of the amorphous In_3SbTe_2 phase change compound, Phys. Rev. B 88 (2013) 174203.
[31] N.F. Mott, E.A. Davis, Electronic Processes in Non-Crystalline Materials, 2nd edition, Oxford University Press, 1979, pp. 460.
[32] Elena F. Bazarkina, Gleb S. Pokrovski, V. Alexander Zotov, Structure and stability of cadmium chloride complexes in hydrothermal fluids, Chem. Geol. 276 (2010) 1–17.
[33] O.V. Aleksandrov, K.V. Kiseleva, S.D. Kuchaev, Khimicheskaya Svyaz' In-Te V Reshetke $Pb_{0.78}Sn_{0.22}Te$, AN SSSR, Moscow. Fizicheskij Inst; Kratkie Soobshcheniya Po Fizike, 1, 1985, pp. 60–63.
[34] E. Mooser, Bonds and bands in semiconductors, in: P.N. Butcher, N.H. March, M.P. Tosi (Eds.), Crystalline Semiconducting Materials And Devices, Springer Science + Business Media, New York, 2017, p. 39.
[35] J.C. Phillips, Bonds Bands in Semiconductors, ACADEMIC Press, New York and London, 1973, pp. 202.
[36] A.J. Rosenberg, A.J. Strauss, Solid solutions of In_2Te_3 in Sb_2Te_3 and Bi_2Te_3, J. Phy. Chem. Solids 19 (1961) 105–116.
[37] B. Legendre, B. Gather, R. Blachnik, Ternary chalcogen-Containing systems - 9 the indium-Antimony-Tellurium system, *Z. Metallkd/Mater. Res. Adv. Tech*. 71 (9) (1980) 588.
[38] Otfried Madelung, Semiconductors Data Handbook, 3rd edition, Springer-Verlag, Berlin Heidelberg, New York, 2004 (286).
[39] Manoj Ducher, Marc Blanchard, Delphine Vantelon, Ruidy Nemausat, Delphine Cabaret, Probing the local environment of substitutional Al3+ in goethite using X-ray absorption spectroscopy and first-principles calculations, Phys. Chem. Miner. 43 (2016) 217–227.